Ferroelastic Nanostructures and Nanoscale Transitions: Ferroics with Point Defects

Xiaobing Ren, Yu Wang, Kazuhiro Otsuka, Pol Lloveras, Teresa Castán, Marcel Porta, Antoni Planes, and Avadh Saxena

Abstract

For decades, a kind of nanoscale microstructure, known as the premartensitic "tweed structure" or "mottled structure," has been widely observed in various martensitic or ferroelastic materials prior to their martensitic transformation, but its origin has remained obscure. Recently, a similar nanoscale microstructure also has been reported in highly doped ferroelastic systems, but it does not change into martensite; instead, it undergoes a nanoscale freezing transition—"strain glass" transition—and is frozen into a nanodomained strain glass state. This article provides a concise review of the recent experimental and modeling/simulation effort that is leading to a unified understanding of both premartensitic tweed and strain glass. The discussion shows that the premartensitic tweed or strain glass is characterized by nano-sized quasistatic ferroelastic domains caused by the existence of random point defects or dopants in ferroelastic systems. The mechanisms behind the point-defect-induced nanostructures and glass phenomena will be reviewed, and their significance in ferroic functional materials will be discussed.

Introduction

Nanoscale structures (hereafter abbreviated as nanostructures), in the form of cross-hatched tweed or mottled morphology, have been reported in a wide range of important functional materials, including ferroelastics (or martensites, shape-memory materials),[1–3] ferroelectrics,[4,5] ferromagnets,[6] superconductors,[7,8] and colossal magnetoresistance (CMR) materials.[9] They are of great interest for understanding the nature and functionalities of these important materials,[10–13] but in many cases, a clear and unified understanding is lacking. This article focuses on the nanostructures in ferroelastics and provides a possible unified explanation based on recent experimental[14–18] and theoretical[19,20] progress on this subject, which advances the earlier understanding.[21–25] We shall also discuss striking similarities in the nanostructure evolution as a function of defect concentration or temperature among different classes of materials, as well as in the corresponding physical properties. This indicates a similar underlying physics controlling the formation of these nanostructures and their behavior. Therefore, the ideas used in ferroelastic systems may be applicable to other ferroic systems, such as ferroelectrics and ferromagnets, and may be extended even to superconductors and CMR manganites.

Ferroelastic materials, or martensitic materials in metallurgical terminology (in this article we shall use both without distinction), are an important class of materials exhibiting interesting functional properties such as shape-memory effect and superelasticity.[26] All the functional properties of these materials are rooted in a displacive transition called ferroelastic or martensitic transition, which involves a long-range ordering of lattice strains below a transition temperature M_s. Such strain ordering causes a symmetry lowering from a high symmetry "parent" phase (normally a cubic phase) into a low symmetry ferroelastic (or martensite) phase (e.g., the B19' monoclinic phase).[25,27] The symmetry breaking gives rise to a characteristic hierarchical pattern of ferroelastic domains in the low-temperature phase that minimizes strain energy generated during the transition.[28,29] The lattice or unit cell distortion involved can be either a homogeneous lattice deformation (like shear) or an intra-cell deformation (like shuffle), or both. Most shape-memory alloys, such as TiNi, involve both shear and shuffle during the martensitic transition.

For ideal ferroelastic/martensitic systems containing no defects (i.e., point defects such as dopants, chemical disorder, or impurities), there exists little mystery for their ferroelastic transition, microstructure, and corresponding macroscopic properties; they are well understood.[25,26] However, actual ferroelastic materials are not perfectly "clean," they invariably contain a certain amount of defects, introduced either inadvertently as impurities or intentionally as dopants or a chemical disorder to modify certain properties. The existence of such defects in these materials creates a long-standing mystery: A nanoscale microstructure[1–3] with a cross-hatched tweed or mottled morphology has been reported in various ferroelastic systems prior to their ferroelastic transitions (i.e., in the parent phase); these nanostructures have been found to persist tens of degrees above the M_s temperature[30,31] and are assumed to be a "precursor phase" of the incoming martensite phase. Information from neutron scattering[1,30] and transmission electron microscopy (TEM)[1,2,30] has indicated that these premartensitic nanostructures are composed of nano-sized, quasistatic ferroelastic domains. The premartensitic nanostructure was found to arise as anisotropic tweed or isotropic mottled morphology depending on the elastic anisotropy of the system. Highly anisotropic systems such as Ni-Al give rise to a tweed microstructure (Figure 1a),[30] whereas more nearly isotropic systems such as TiNi-based alloys result in a

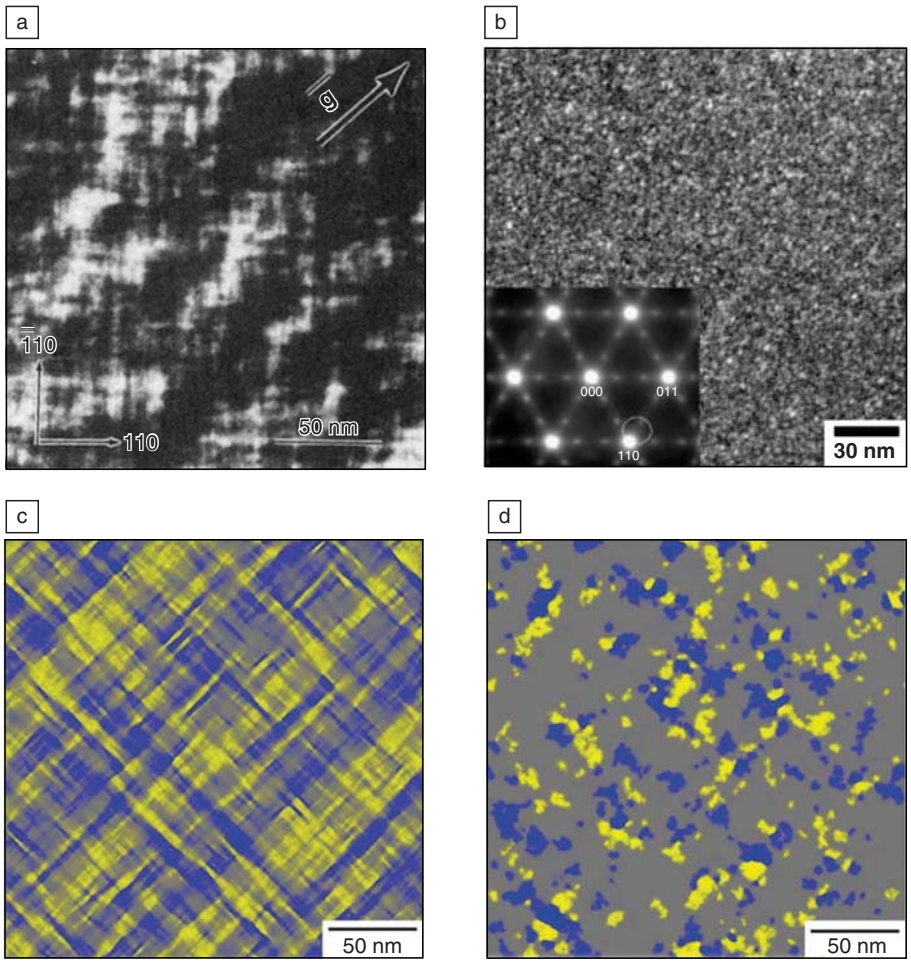

Figure 1. Two forms of premartensitic nanostructures and the relation to elastic anisotropy. (a) Experimentally observed tweed in Ni-Al with high anisotropy.[1] (b) Experimentally observed mottled structure in TiNiFe.[2] (c) Simulated tweed with high anisotropy. (d) Simulated mottled structure with low anisotropy.

mottled microstructure (Figure 1b)[2] prior to the martensitic transition. Simulation results are shown in Figure 1c and 1d for high and low anisotropy, respectively. They will be explained later in this article. The biggest mystery about these premartensitic nanostructures is why a nano-sized ferroelastic phase can exist in a temperature range (i.e., the parent state), where it is apparently thermodynamically unstable. It also remains unclear how elastic anisotropy affects the morphology of the premartensitic nanostructures.

Early theoretical studies[21–25] in the 1990s made an important first step toward an understanding of the premartensitic nanostructures. These studies have indicated that random point defects are responsible for the formation of the premartensitic tweed. The random distribution of point defects causes a spatial distribution in the local M_s temperature, thereby some local regions can transform into the martensite at a temperature well above the nominal M_s temperature of the whole system.[21] In this way, nano-sized martensite domains, which show up as the tweed, appear above the M_s temperature. These studies also suggested that the tweed pattern results from a frozen state of ferroelastic strains, such as a spin glass (a frozen disordered spin state), but the suggested glassy state of the tweed has now been confirmed by experiment.[18]

Recently, a new kind of nanoscale mottled microstructure has been reported in the well-known ferroelastic system, $Ti_{50-x}Ni_{50+x}$, when the point defect (excess Ni) concentration x exceeded a critical value (x > 1.3 mol%).[14–18] (Such compositions had been known as nontransforming compositions but showed an abnormal negative temperature coefficient in electrical resistivity.[32]) Although the mottled structure has a similar appearance to the premartensitic mottled structure shown in Figure 1b, this new nanostructure does not transform into martensite, unlike the premartensitic nanostructure; instead, it keeps a mottled nanostructure down to the lowest temperature achievable.[14] Extensive experimental studies on the new nanostructure system have revealed that such a system undergoes a freezing of local strains at a glass transition temperature T_g.[14,16] Such a glass transition is termed "strain glass transition," and the low-temperature state of the nanostructure corresponds to a frozen strain glass, which is a frozen state of disordered lattice distortion or simply a nano-sized martensite.[14] Recent numerical simulations of a Landau-Ginzburg type model (a model calculating free energy as a function of strain order parameter, which varies in space)[19,20] have demonstrated the crucial role of point defects (or inhomogeneities) in the formation of strain glass, and it further demonstrates that the elastic anisotropy plays a key role in determining whether the nanostructure appears as tweed or mottled morphology.

Then a central question arises: Is there a unified explanation for both premartensitic nanostructure and the similar nanostructure of strain glass? In view of the recent progress in experimental studies[14–18] on strain glass and in the modeling of the premartensitic nanostructures,[19–24] it seems possible to provide such an answer. In the following, we shall combine both experimental findings with recent modeling and simulation results to provide a general understanding of the origin of nanoscale microstructures. The ideas also may be applicable to similar phenomena in a wide range of ferroic materials and other functional materials, such as high-T_c superconductors and CMR materials. Strain glass, as a new horizon of ferroelastic research, may offer opportunities for both fundamental and applied studies. The physics of the glass behavior may enrich the current theory of ferroelasticity. Strain glass has been shown to exhibit a number of interesting properties, such as shape-memory effect and superelasticity,[15] and many others yet to be discovered.

Crossover from Martensitic Transition to Strain Glass Transition: Premartensitic Nanostructure Versus Strain Glass Nanostructure?

Figure 2a shows the phase diagram of $Ti_{50-x}Ni_{50+x}$ (x is the concentration of excess Ni as point defects),[14] where microscopic features of all phases are shown in the inset micrographs. The most notable feature of this phase diagram is that there

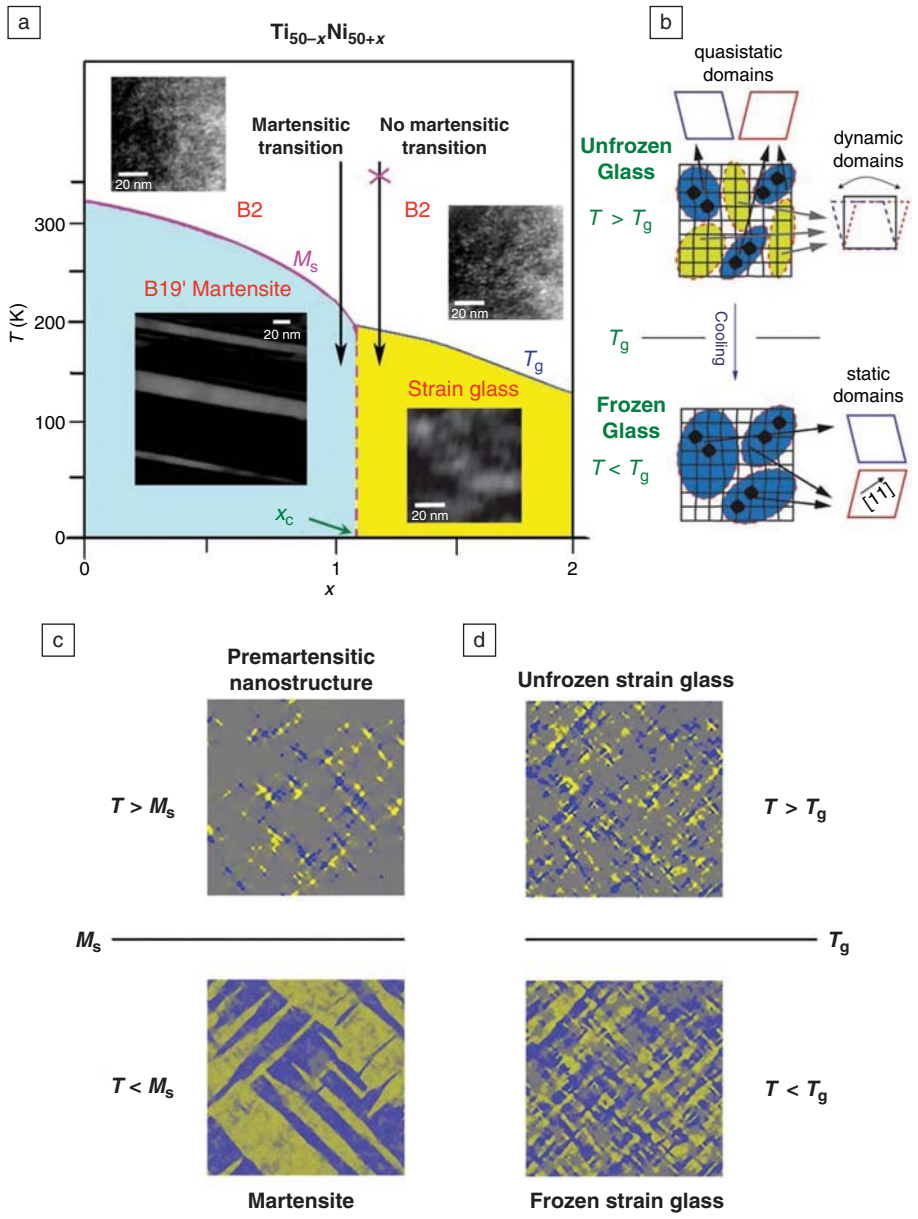

Figure 2. Crossover from a normal martensitic transition to a strain glass transition by point defect doping in the $Ti_{50-x}Ni_{50+x}$ system, where x is the concentration of point defects (excess Ni). (a) Phase diagram showing the normal martensitic transition for $x < x_c$ and strain glass transition at $x > x_c$.[14] The corresponding microstructures (or nanostructures) of the high- and low-temperature phases (B2, B19', strain glass) are embedded. B2 is a CsCl structure; B19' is a monoclinic structure. (Image courtesy of S. Sarkar). (b) Schematic microscopic picture of unfrozen ($T > T_g$) and frozen ($T < T_g$) strain glass. Unfrozen strain glass shows essentially dynamic domain flipping but quasistatic nanodomains also exist. Frozen strain glass exhibits essentially static nanodomains only. (c) Simulated premartensitic nanostructure to normal martensite transition at low defect concentration (intermediate anisotropy). (d) Simulated strain glass transition at higher defect concentration (with the same anisotropy). T, temperature; T_g, glass transition temperature.

exists a point-defect-induced crossover from a normal martensitic transition to a strain glass transition (explained later in article) at a critical defect concentration $x_c \sim 1.3$. (Note that the most accurate measurements from Reference 14 found $x_c \sim 1.1$, as shown in Figure 2a, but the phase diagram is sufficient for illustrative purposes.) This phase diagram reveals the different transformation behaviors of premartensitic nanostructure (for $x < x_c$) and strain glass nanostructure (for $x > x_c$). Such a phase diagram is expected to be generic for many ferroelastic systems, and it can provide an ideal arena for understanding the transformation behavior of defect-containing ferroelastic systems, in particular the effect of point defects. In the following, we shall discuss the normal martensitic transition (for $x < x_c$) and strain glass transition (for $x > x_c$) separately and describe their corresponding nanoscale microstructures. Based on the experimental observations discussed in the next section we shall discuss the relation between the two kinds of nanostructures and answer the key questions raised in the introduction.

Normal Martensitic Transition for $x < x_c$ and the Associated Premartensitic Nanostructures

For $x < x_c$, the NiTi system undergoes a normal martensitic transition from B2 (cubic) parent phase to B19' (monoclinic) martensite. In the parent state ($T > M_s$), the parent phase is not an ideal, homogeneous B2 phase, rather it shows a mottled or spotted premartensitic nanostructure. During the martensitic transition temperature, the premartensitic nanostructure changes drastically into large, regular martensitic twins at $T < M_s$, as shown in the corresponding micrographs in Figure 2a (for $x < x_c$). The mottled or spotty premartensitic nanostructure of Ti-Ni corresponds to the very low elastic anisotropy ($A \sim 2$) of this system.[2] Here $A = C_{44}/C'$ and is the ratio of the shear modulus to the deviatoric modulus. On the other hand, most martensitic systems exhibit high elastic anisotropy,[33] and in such cases, the premartensitic nanostructure is characterized by a cross-hatched tweed morphology, as in Figure 1a. The morphology feature (tweed or mottled) of premartensitic nanostructures and its relation to elastic anisotropy will be explained later.

Previous TEM studies[1,2,30] have demonstrated that premartensitic nanostructures are (quasi-) static martensite domains. They may have either a similar structure (but with less lattice distortion) as the low-temperature martensite phase or an alternative candidate structure of the low-temperature martensite.[33] For example, in the Ni-Al system, the premartensitic structure and the low-temperature martensite have similar structures.[30] On the other hand, in TiNi and TiNiFe systems, the premartensitic structure has a rhombohedral (R)-like structure,[2,34] being different from the B19' (monoclinic) martensite at low temperature. Nevertheless, as the R phase is another candidate martensite phase for this system,[33] it is not surprising to have this structure as a premartensitic state.

Because the premartensitic nanostructure does not possess long-range order, the diffraction peaks are usually not located at the exact commensurate positions expected for a fully developed long-range ordered martensite phase. Therefore, the premartensitic nanostructure often appears, from the diffraction pattern, as if it is an incommensurate phase. This explains the experimental reports of the "incommensurate" premartensitic state.[33,34]

It should be noted that the quasistatic premartensitic nanostructure corresponds to a "central peak" or "elastic peak" (the zero energy-loss peak) in neutron inelastic scattering experiments.[30] The temperature dependence of the central peak in various martensitic systems seems to suggest that the premartensitic nanostructure and the associated static lattice distortion gradually fade away with increasing temperature over a temperature range as wide as 50–200 K, and the gradual change from a premartensitic state to an ideal B2 (CsCl structure) state is not a thermodynamic phase transition, as there exists no anomaly in any physical property.[18]

An intriguing question arises as to whether or not the premartensitic nanostructure also exists in a defect-free system. Neutron inelastic scattering on Zr has found that for pure Zr, the central peak vanishes, but oxygen-doped Zr shows a central peak.[35] As the central peak corresponds to the quasistatic nanodomains in the TEM pictures, the vanishing central peak in high-purity samples suggests that the defect-free parent phase does not show a quasistatic nanostructure prior to the martensitic transformation. It has also been found that for the $Ti_{50-x}Ni_{50+x}$ system, with $x \to 0$, the stoichiometric TiNi shows no diffuse 1/3 spots (i.e., no R-like nanodomains).[36] Therefore, available experimental observations seem to suggest that there are no static premartensitic nanostructures prior to martensitic transition.

Nanoscale Transition (Strain Glass Transition) for $x > x_c$ and the Associated Strain Glass Nanostructures

For $x > x_c$, the martensitic transition vanishes, and instead a nanoscale transition called the strain glass transition takes place.[14] The strain glass transition is characterized by the freezing of nano-sized ferroelastic domains at freezing temperature T_g (shown in the right insets of Figure 2a, and schematically shown in Figure 2b), similar to a cluster spin glass transition or a ferroelectric relaxor transition. These nanodomains also originate from the random point defects (or dopants), being the same as the premartensitic nanostructures, but strain glass contains a higher defect concentration. The strain glass transition, being different from a martensitic transition, involves two seemingly contradictory signatures: (1) invariance of the average structure through T_g (Figure 3a) and (2) the existence of a frequency-dependent anomaly at the glass transition temperature T_g (Figure 3b) following a Vogel-Fulcher relation, a relation between T_g and frequency that describes the dynamic freezing process.[14,15] At $T > T_g$, the nano-sized ferroelastic domains dynamically flip as a whole (as evidenced by softening of the phonons), but there are a number of long-lived, quasistatic nanodomains (Figure 2b, $T > T_g$). These quasistatic nanodomains can be imaged by TEM as the mottled nanostructure (Figure 2a, inset figure in the strain glass regime). With temperature decreasing, the nanodomains grow to some extent but are eventually frozen below T_g; thus, we can see bigger nanodomains at $T < T_g$ (Figure 2b). Therefore, a strain glass transition involves a freezing transition from a dynamically disordered strain state (i.e., strain liquid) to a frozen disordered strain state (strain glass). This is analogous to the formation of a jelly (structural glass) from a gelatin water solution (defect-containing liquid) during cooling. A TEM image of the unfrozen strain glass and its corresponding frozen glass can be found in Figure 2a (the inset in the strain glass regime) for the $x > x_c$.

The most important information from Figure 2a is that point defects can induce a crossover from normal martensitic transition to strain glass transition at a critical concentration x_c. Below x_c, the martensitic transition remains, but the transition temperature is lowered with increasing defect concentration; above x_c, the martensitic transition is absent, and instead the system undergoes a freezing transition of the

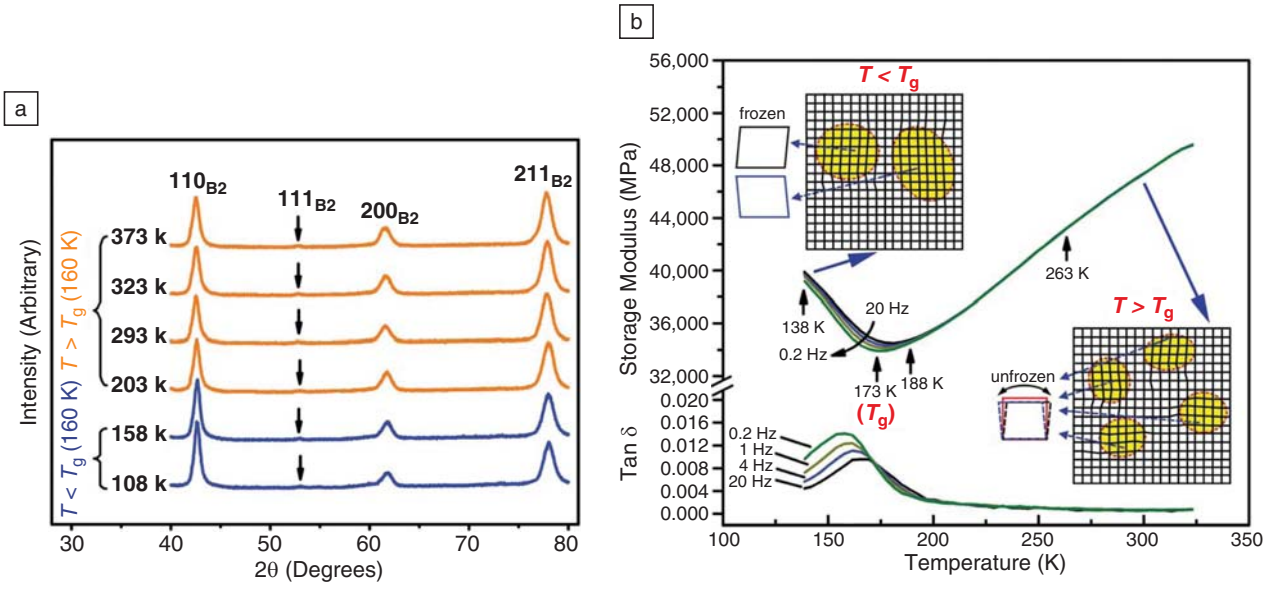

Figure 3. Signatures of strain glass transition: (a) invariance in average structure, and (b) anomaly in ac mechanical susceptibility at the glass transition temperature T_g. The storage modulus is the inverse of the mechanical susceptibility. Tan δ is the loss; δ is the phase angle between stress and strain during dynamical mechanical testing. The insets show the microscopic pictures of nanodomains, essentially ergodic at $T > T_g$ and non-ergodic at $T < T_g$. The different orientations of the parallelograms represent different strain states.[15] T, temperature.

nanodomains, the strain glass transition. The strain glass transition does not involve a change in average structure, thus it cannot be detected by x-ray diffractometry; but dynamical mechanical measurement can clearly reveal such a transition.

Historically, it has been found for a long time that the martensitic transition seems to vanish suddenly if the doping level exceeds a certain level, but it was generally assumed that this is caused by the very low thermodynamic stability of martensite at such a high doping level. However, these "non-martensitic" alloys (e.g., $Ti_{50-x}Ni_{50+x}$ with $x > 1.3$) were found to exhibit abnormal physical properties, such as a negative temperature coefficient of electrical resistivity,[32] but the origin remained unclear. With the discovery of the strain glass transition in such alloys,[14] the previous puzzle can now be solved. The "negative temperature coefficient" of electrical resistivity is simply a result of the gradual growth of the nanodomains with an R-like structure, which has a higher specific resistivity.[33]

A critical proof for the glass transition is the existence of non-ergodicity, or history dependence of the physical properties (such as strain) in the glass state. This is usually done with a field-cooling and zero-field-cooling (FC/ZFC) experiment, which detects if there is a history dependence of the physical properties. Figure 4a shows the FC/ZFC curves of the strain glass $Ti_{48.5}Ni_{51.5}$.[16] It is clear from the deviating FC and ZFC curves below T_g that the system is ergodic at $T > T_g$ and becomes non-ergodic at $T < T_g$. (Strictly speaking, a small deviation actually begins above T_g, indicating a slight ergodicity breaking.) This proves that this system indeed undergoes a strain glass transition. It is noted that the FC/ZFC behavior of the strain glass shows a striking similarity with that of two other kinds of glass transitions, the relaxor ferroelectric transition (freezing of local electric dipoles) (Figure 4c) and the cluster spin glass transition (a freezing of magnetic moments) (Figure 4d). As strain glass, relaxor, and cluster spin glass are derived from three ferroic transitions (i.e., ferroelastic transition, ferroelectric transition, and ferromagnetic transition, respectively), these three glasses can be generalized into one bigger class of glasses—the ferroic glasses. They exhibit very similar behavior in their corresponding dc and ac properties.

Strain glass exhibits a number of unexpected properties such as shape-memory effect and superelasticity.[15] As a strain glass does not undergo a martensitic transition and looks like a nontransforming, "dead" material, there seems no reason to have a shape-memory effect, which characterizes only a martensitic system. However, as can be seen from Figure 5a, a strain glass (T_g ~ 168 K) can also exhibit a shape-memory effect (when deformed at $T < T_g$ and heated up to $T > T_g$, the blue curve), very similar to a normal martensitic alloy. It is further found that at $T > T_g$, a strain glass can also exhibit superelasticity (the 173 K and 188 K curves). The unexpected shape-memory effect of strain glass can be explained by the formation of long-range strain order (martensite) by external stress and its recovery to the initial unfrozen strain glass state.[15] Figure 5b shows the simulation results about the stress-strain curve of the frozen glass. The details will be explained in the next section.

Relationship Between the Premartensitic Nanostructure and the Unfrozen Strain Glass Nanostructure

In Figure 2a, the two kinds of nanostructures, the premartensitic nanostruc-

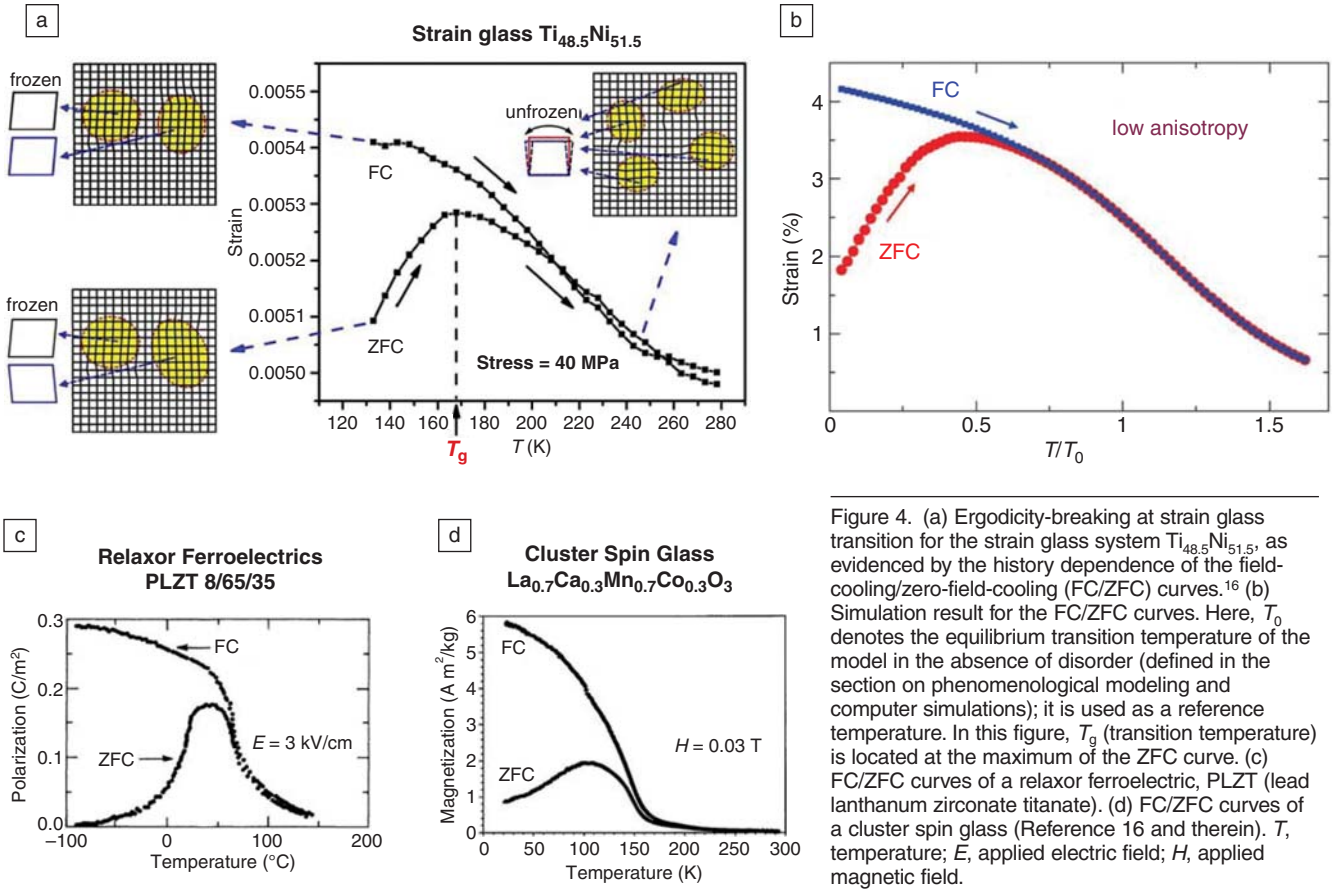

Figure 4. (a) Ergodicity-breaking at strain glass transition for the strain glass system $Ti_{48.5}Ni_{51.5}$, as evidenced by the history dependence of the field-cooling/zero-field-cooling (FC/ZFC) curves.[16] (b) Simulation result for the FC/ZFC curves. Here, T_0 denotes the equilibrium transition temperature of the model in the absence of disorder (defined in the section on phenomenological modeling and computer simulations); it is used as a reference temperature. In this figure, T_g (transition temperature) is located at the maximum of the ZFC curve. (c) FC/ZFC curves of a relaxor ferroelectric, PLZT (lead lanthanum zirconate titanate). (d) FC/ZFC curves of a cluster spin glass (Reference 16 and therein). *T*, temperature; *E*, applied electric field; *H*, applied magnetic field.

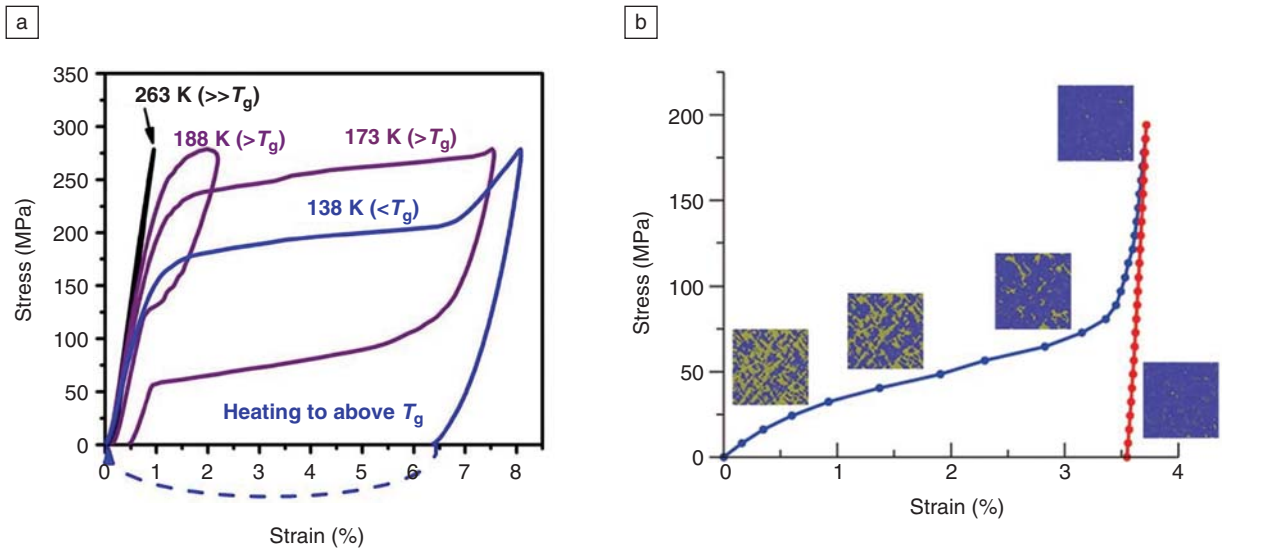

Figure 5. (a) Experimental results on the shape-memory effect (plastic deformation at $T < T_g$ and the shape recovery at $T > T_g$) and superelasticity (deformation at $T > T_g$) of strain glass $Ti_{48.5}Ni_{51.5}$. (b) Simulation results for plastic deformation at low temperature. Insets show snapshots of configurations at a given value of strain. The image size is scaled down by a factor of five as compared to Figure 1c and 1d. *T*, temperature.

ture ($x < x_c$, $T > M_s$) and the nanostructure of unfrozen strain glass ($x > x_c$, $T > T_g$), look very similar; both exhibit quasistatic nanodomains with a ferroelastic structure. The only difference is that the unfrozen strain glass nanostructure corresponds to a higher defect concentration; this leads to a smaller nanodomain size. Recent studies with FC/ZFC and mechanical susceptibility experiment showed that both types of nanostructures have similar ergodic behavior, but a small history dependence still exists.[18] This means that both nanostructures correspond to essentially a "strain liquid" state (i.e., ergodic), but the liquid has a certain "stickiness" (i.e., a quasistatic component exists). The nanostructure of the unfrozen strain glass ($T > T_g$) corresponds to a stickier state than the premartensitic nanostructure.[18] Quantitative analysis of the dynamics of the strain glass has shown that extremely long-time relaxation (>10^3 seconds) exists in the unfrozen glass state ($T > T_g$).[37] This long-lived strain fluctuation or quasistatic component in the more viscous strain liquid corresponds to the "static" nanostructure observed by TEM. This picture is also true for the premartensitic nanostructure, but it is less viscous. Therefore, there is no fundamental difference in physical nature between the premartensitic nanostructure ($x < x_c$) and the nanostructure of the unfrozen strain glass ($x > x_c$); both correspond to a more viscous strain liquid state, but a higher defect concentration makes an even more viscous strain liquid. This is very similar to an everyday phenomenon: adding more gelatin into water will make a more viscous liquid, and at high gelatin doping, the viscous liquid does not freeze into the crystal ice, rather it is frozen into a structural glass—jelly. The difference in viscosity results in different consequences: the less-viscous strain liquid ($x < x_c$) undergoes a normal martensitic transition, but the viscous liquid ($x > x_c$) undergoes a freezing transition into a strain glass. Point defects are responsible for such a crossover.[18]

Phenomenological Modeling and Computer Simulations of Premartensitic Nanostructures and Strain Glass Nanostructures

Different phenomenological models have been proposed to account for nanoscopic textures in ferroelastic and martensitic materials. All of these models incorporate the requirements that the system must sensitively respond to local coupling to some kind of disorder.[21–25] The model used here[19,20] is a generalization of the model proposed by Kartha et al.[21] It successfully reproduces the experimentally observed premartensitic nanostructures and strain glass structures. In particular, it explains why some systems exhibit a tweed nanostructure, whereas others exhibit a mottled or spotty nanostructure.

The model has the following key features: (1) The free energy of the system is described by a Landau-Ginzburg energy function extended to consider long-range elastic interactions. This model describes a defect-free ferroelastic transition and the resultant domain morphology. (2) Random point defects (or inhomogeneities) are assumed to cause a spatial distribution of M_s temperatures over the system. Some details of the model are given later.

Given that the inhomogeneous strain fluctuations of interest here are confined into certain (two-dimensional) planes,[25] we shall illustrate the problem for a 2D square-to-rectangle transition that mimics a cubic-tetragonal transition (where the rectangular cross-section of the tetragonal phase is used in 2D). Suppose that e_1, e_2, and e_3 are the symmetry-adapted strains representing, respectively, hydrostatic, deviatoric, and shear distortions of the cubic lattice. The change of symmetry at the transition is described by e_2, which will be the (primary) order parameter e_2. Soft directions will be along $\{11\}\langle 1\bar{1}\rangle$ displacements corresponding to a small elastic constant C', defined as

$$C' = (C_{11} - C_{12})/2, \quad (1)$$

where C_{11} and C_{12} are, respectively, the components C_{xxxx} and C_{xxyy} of the second-order elastic constant tensor. The elastic anisotropy is then measured by the ratio $A = C_{44}/C'$ (where C_{44} is the component C_{xyxy} of the elastic constant tensor associated with shear distortions). A general Landau free-energy density for this transition will be of the form

$$F = F_h + F_{grad}, \quad (2)$$

where the first term is the homogeneous contribution adequate for a first-order transition, which includes both the nonlinear contribution associated with the primary order parameter (e_2) and the harmonic elastic energy associated with nonsymmetry breaking strains, nonorder parameter strain components, (e_1, e_3). The second term is a gradient (or Ginzburg) term accounting for the energy cost of interfaces, such as twin boundaries. When this free energy is minimized, imposing the requirement of smoothly fitting unit cells without creating (structural) defects by means of the elastic compatibility (Saint-Vénant) condition,[29] the dependence on the nonsymmetry breaking strains gives rise to a nonlocal, long-range anisotropic interaction. Here, it is denoted by the function $U(\boldsymbol{r}-\boldsymbol{r}')$ that correlates any two unit cells at positions r and r', respectively.[28] The following free energy density is obtained:

$$F = C'(T,\eta)\, e_2^2 - B\, e_2^4 + D\, e_2^6 + K\, |\nabla e_2|^2 + d\boldsymbol{r}'\, e_2(\boldsymbol{r})\, U(\boldsymbol{r}-\boldsymbol{r}')\, e_2(\boldsymbol{r}'). \quad (3)$$

T is the temperature, η the disorder field, and B, D, and K are phenomenological parameters.

In this model, point defects are taken into account by means of a quenched-in, spatially fluctuating field included in the harmonic coefficient C', which is assumed to be of the form

$$C'(T,\eta(\boldsymbol{r})) = a[T - T_c - \eta(\boldsymbol{r})], \quad (4)$$

where T_c is the lower stability limit of the high-temperature phase in the clean (absence of disorder) limit, and a is defined by Equation 4 and is the temperature derivative of C'. Usually, the disorder field η is assumed to be spatially correlated and Gaussian distributed with zero mean. Thus, disorder has the effect of producing a distribution of transition temperatures $T(\boldsymbol{r}) = T_0 + \eta(\boldsymbol{r})$, where T_0 is the equilibrium transition temperature of the model in the clean limit. Therefore, regions with different degrees of metastability separated by finite free energy barriers exist in the system. In the previous expression, the long-range kernel $U(\boldsymbol{r}-\boldsymbol{r}')$ goes as $A\cos(4\theta)/|\boldsymbol{r}-\boldsymbol{r}'|^2$. This term is essential to providing a global response due to a local coupling of strain to disorder, which is necessary for textures to occur. Note that this long-range term is minimized for a cross-hatched (tweed) pattern due to the $\cos(4\theta)$ leading term.

This means that order parameter correlations will be favored along the {11} diagonal directions ($\theta = \pm\pi/4$). However, since the strength of this long-range interaction is controlled by the anisotropy factor A, these correlations along the diagonals will be strongly screened for low enough values of the elastic anisotropy. It was previously demonstrated that in the limit of infinite elastic anisotropy, this model can be exactly mapped to a random-bond version of the antiferromagnetic spin-glass Sherrington-Kirkpatrick model.[21]

In the following, we summarize a number of key results reported in References 19 and 20 that arise from the numerical simulations of the present model and compare them with the experimental data when available. We shall find that the simulation results are in good agreement with experiments.

(1) Static premartensitic nanostructures are absent in a defect-free (i.e., $\eta(\boldsymbol{r}) = 0$) ferroelastic system.

(2) Static premartensitic nanostructures exist only in a defect-containing system (i.e., $\eta(\boldsymbol{r}) \neq 0$) prior to the martensitic transition. The value of elastic anisotropy $A = C_{44}/C'$ determines the morphology of the premartensitic nanostructures. High anisotropy leads to cross-hatched premartensitic tweed (Figure 1c) before the martensitic transition; low anisotropy results in a mottled/spotty nanostructure (Figure 1d) prior to the transition. This is in good agreement with the experimental results shown in Figure 1a (high anisotropy) and Figure 1b (low anisotropy).

(3) There exists a crossover at a critical defect concentration x_c, from a normal martensitic transition into a freezing transition of the nano-sized ferroelastic domains—the strain glass transition. Figure 2c and 2d show the simulation results for an intermediate anisotropy system (such as NiTi(Fe) with low Fe content) with low and high defect concentration, respectively. At low defect concentration ($x < x_c$), the system undergoes a normal martensitic transition from a premartensitic nanostructure (spotty domains) to a normal martensite with large twins (Figure 2c). At high defect concentration ($x > x_c$), the normal martensitic transition vanishes, and instead the system exhibits a freezing transition during which the system retains the nanodomains down to 0 K (Figure 2d). The simulated results in Figure 2c and 2d reproduce the crossover from the normal martensitic transition into the nanoscale transition of strain glass.

(4) The proof that the nanoscale transition shown in Figure 2d is a strain glass transition can be found in Figure 4b. The calculated FC/ZFC curves show a characteristic history dependence below T_g, which should correspond approximately to the temperature of the maximum of the ZFC curve in Figure 4b. The deviation between both FC and ZFC curves is indicative that the nanoscale transition shown in Figure 2d is indeed a strain glass transition. This simulation result is in good agreement with the experimental one for $Ti_{58.5}Ni_{51.5}$ (Figure 4a). No signatures of glassy behavior have been observed in the premartensitic nanostructure (Figure 2c), which transforms into a long-range twinned martensitic state. This is also in agreement with experimental observation.[18]

(5) External stresses can change a strain glass with nanodomains into normal martensite with large domains or even a single domain, as shown in Figure 5b. The presence of a stress favors a particular strain domain and at the same time overcomes the energy barrier for domain switching. As a result, the nano-sized multi-domains of the frozen strain glass are switched into a favorable single domain of a normal martensite. With heating to a temperature above T_g, the system reverts to the nanodomained state with average cubic structure (such as Figure 2d, the state at $T > T_g$). This causes a recovery of the original sample shape and leads to the shape-memory effect. Depending on temperature, superelastic or pseudoelastic (plastic) behavior is found. Such a result is in good agreement with the experimental one shown in Figure 5a.

(6) Elastic anisotropy can affect the critical defect concentration for the crossover from a normal martensitic transition to a strain glass transition, as shown in Figure 6. High anisotropy (A) requires a high defect concentration (accounted for in the model by a high enough amount of disorder) to render the system into a strain glass, and lower

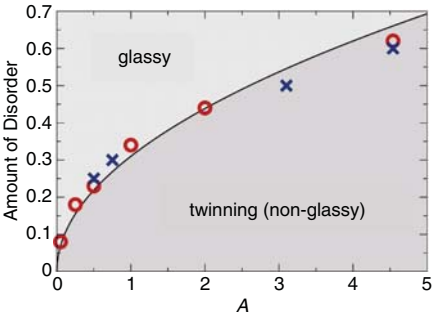

Figure 6. The influence of elastic anisotropy A on the critical amount of disorder (point defects) to induce a crossover from a normal martensite (twinning) to a strain glass state.[19,20] The values denoted by circles have been computed from the FC/ZFC curves, whereas the values denoted by crosses have been obtained from the free-energy metastability analysis. For more details, see Reference 20.

anisotropy requires a lower critical defect concentration (amount of disorder) to make a strain glass. The reason for this effect is that high anisotropy increases the strength of the long-range elastic interaction and hence favors a long-range strain ordering (i.e., the normal martensitic transition).

Generic Phase Diagram for Point-Defect-Containing Ferroic Systems—Crossover from Ferroic Transition to Ferroic Glass Transition

A ferroelastic (or martensitic) transition, a ferroelectric transition, and a ferromagnetic transition involves long-range ordering of lattice distortion (or strain), electric dipole, and magnetic moment, respectively. The long-range interaction arises from elastic compatibility (i.e., elastic dipoles), electric dipoles, and magnetic dipoles, respectively. Except for a difference in the order parameter, the behavior of these ordering transitions and the associated microstructures, as well as physical properties, are very similar or parallel. Thus they are called ferroic transitions as a whole.[38]

An appealing question arises as to whether point defects (or inhomogeneities) in these different systems can generate similar consequences as those for ferroelastic systems (shown in the phase diagram of Figure 2a). The answer is yes, and it seems that point defects can produce strikingly similar consequences for these ferroic systems (Figure 2a),[39,40] but such similarity has not been generally acknowledged in the past.

For ferroelastic systems, we have known from the previous discussion that point defects produce two prominent consequences: (1) Below a critical defect concentration ($x < x_c$), the normal ferroelastic or martensitic transition remains, but the defects cause the formation of a premartensitic nanostructure above the transition temperature. (2) Above the critical defect concentration ($x > x_c$), long-range strain ordering (ferroelastic transition) is suppressed; instead, a nanoscale freezing transition, the strain glass transition, takes place.

For ferroelectric systems, low-level doping does not suppress the ferroelectric transition but causes a static short-range ordering of electric dipoles above the ferroelectric transition temperature T_c. Such short-range ordering corresponds to the nano-sized ferroelectric domains above the transition temperature and can extend to a rather high temperature.[41] On the other hand, a high concentration of suitable dopants (as point defect) can create a glassy phase called a relaxor, where nano-sized dipolar domains are frozen below a freezing temperature T_g.[39] Therefore, there exists a crossover from a normal ferroelectric transition into a relaxor (glass) transition at a critical defect concentration,[41] being similar to its ferroelastic counterpart.

For ferromagnetic systems, a similar situation exists. It has been known for a long time that doping with a sufficiently high concentration of nonmagnetic elements (as point defects) can destroy the long-range magnetic order of a ferromagnetic system, resulting in a locally ordered state called cluster spin glass.[40] But little is known about whether there is a "precursor nanostructure" prior to the normal ferromagnetic transition for insufficient doping. Fortunately, a magnetic precursor nanostructure (called "magnetic tweed") recently has been discovered,[6,42] and a theoretical model has been established.[6] Again, we find a very similar situation as the other two classes of ferroic materials.

From the previous discussion, we can see a beautiful, common picture emerging about the effect of point defects on the three kinds of ferroic materials, as shown in Figure 7. Below a critical defect concentration x_c, the normal ferroic transition is maintained, but in the high-temperature phase, there is short-range ordering (manifesting itself as quasistatic nanostructure or tweed). Above the critical defect concentration x_c, the system crosses over into a ferroic glass transition, where the local ferroic order is frozen below the glass transition temperature T_g; the resultant ferroic glass is a nanostructure of ferroic domains.

Finally, similar nanostructures caused by point defects seem to exist in an even wider range of transforming materials, including many strongly correlated systems such as high-T_c superconductors and CMR manganites;[7–9] the corresponding glass phases are also expected. Indeed, tweed has been reported in yttrium-barium-copper-oxide (YBCO) superconductors, and there exists a critical doping level above which the system shows a tweed-only state with the absence of a normal tetragonal-orthorhombic transition.[7,8] It is highly likely that this tweed-only state is a strain glass. Therefore, the nanostructures and related glass phenomena due to point defects are expected to be a common feature for a wide range of transforming systems, including CMR[9] and possibly multiferroic materials. Exploration of the new physics and novel properties involved is expected to be a very promising area of materials research.

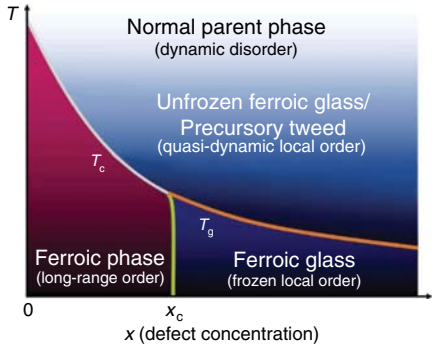

Figure 7. Generic phase diagram of a defect-containing ferroic system showing the crossover from a ferroic transition to a ferroic glass transition. T_c is the transition temperature of the normal ferroic transition; T_g is the glass transition temperature; and x_c is the crossover defect concentration.[18] It is noted that this phase diagram can be applied to ferroelastic, ferroelectric, and ferromagnetic systems. x is the defect concentration.

Conclusions

The physics of undoped or defect-free ferroelastic or martensitic materials is, in general, transparent, and all the microstructural features as well as the physical properties have been almost fully understood. However, when such systems contain point defects or dopants, many puzzling phenomena appear, such as the well-observed premartensitic nanostructures and the recently discovered strain glass—a kind of nanoscale transition. Understanding such phenomena is of fundamental interest and may lead to novel applications. We have reviewed the recent progress in this emerging field and demonstrated that there is a beautiful common picture about the effect of point defects, which create premartensitic nanostructures below a critical level and strain glass above the critical level. The picture may be common among all ferroic systems containing point defects, such as relaxor ferroelectrics and ferromagnets, and similar phenomena may also be found in an even wider range of transforming materials, such as high-T_c superconductors and colossal magnetoresistance manganites.

Acknowledgments

We thank T. Lookman, D. Sherrington, T. Suzuki, D. Wang, Y.Z. Wang, Z. Zhang, and Y.M. Zhou for discussions and S. Sarkar for providing some of the micrographs of Figure 2a. X. Ren and Y. Wang acknowledge the support from JSPS of Japan. A. Planes, T. Castán, and P. Lloveras acknowledge the financial support from CICyT (Spain), Project No. MAT2007-61200, Marie-Curie RTN

MULTIMAT (EU), Contract No. MRTN-CT-2004-505226, and DURSI (Catalonia), Project No. 2005SGR00969. A. Saxena acknowledges the JSPS Invitational Fellowship at Tsukuba, Japan. This work was supported, in part, by the U.S. Department of Energy.

References

1. L.E. Tanner, D. Schryvers, S.M. Shapiro, *Mater. Sci. Eng. A* **127**, 205 (1990).
2. Y. Murakami, H. Shibuya, D. Shindo, *J. Microsc.* **203**, 22 (2001).
3. T. Castán, E. Vives, L. Mañosa, A. Planes, A. Saxena, in *Magnetism and Structure in Functional Materials,* A. Planes, L. Mañosa, A. Saxena, Eds., (Springer Verlag, Berlin, 2005), pp. 27–48.
4. X.H. Dai, Z. Xu, D. Viehland, *Philos. Mag. A* **70**, 33 (1994).
5. X.H. Dai, Z. Xu, J.F. Li, D. Viehland, *Philos. Mag. A* **74**, 395 (1996).
6. A. Saxena, T. Castán, A. Planes, M. Porta, Y. Kishi, T.A. Lograsso, D. Viehland, M. Wuttig, M. De Graef, *Phys. Rev. Lett.* **92**, 197203 (2004).
7. W.W. Schmahl, A. Putnis, E. Salje, P. Freeman, A. Graeme-Barber, R. Jones, K.K. Singh, J. Blunt, P.P. Edwards, J. Loram, K. Mirza, *Philos. Mag. Lett.* **60**, 241 (1989).
8. Y.W. Xu, M. Suenaga, J. Tafto, R.L. Sabatini, A.R. Moodenbaugh, P. Zolliker, *Phys. Rev. B* **39**, 6667 (1989).
9. F. Millange, V. Caignaert, B. Domengès, B. Raveau, E. Suard, *Chem. Mater.* **10**, 1974 (1998).
10. N. Mathur, P. Littlewood, *Nat. Mater.* **3**, 207 (2004).
11. K.H. Ahn, T. Lookman, A.R. Bishop, *Nature* **428**, 401 (2004).
12. E. Dagotto, *Science* **309**, 257 (2005).
13. A.R. Bishop, T. Lookman, A. Saxena, S.R. Shenoy, *Europhys. Lett.* **63**, 289 (2003).
14. S. Sarkar, X. Ren, K. Otsuka, *Phys. Rev. Lett.* **95**, 205702 (2005).
15. Y. Wang, X. Ren, K. Otsuka, *Phys. Rev. Lett.* **97**, 225703 (2006).
16. Y. Wang, X. Ren, K. Otsuka, A. Saxena, *Phys. Rev. B* **76**, 132201 (2007).
17. Y. Wang, X. Ren, K. Otsuka, A. Saxena, *Acta Mater.* **56**, 2885 (2008).
18. X.B. Ren, Y. Wang, Y. Zhou, Z. Zhang, D. Wang, G. Fan, K. Otsuka, T. Suzuki, Y. Ji, J. Zhang, Y. Tian, S. Hou, X. Ding, *Philos. Mag.* (2009), in press.
19. P. Lloveras, T. Castán, M. Porta, A. Planes, A. Saxena, *Phys. Rev. Lett.* **100**, 165707 (2008).
20. P. Lloveras, T. Castán, M. Porta, A. Planes, A. Saxena, *Phys. Rev. B* **80**, 054107 (2009).
21. S. Kartha, T. Castán, J.A. Krumhansl, J.P. Sethna, *Phys. Rev. Lett.* **67**, 3630 (1991).
22. S. Kartha , J.A. Krumhansl, J.P. Sethna, L.K. Wickham, *Phys. Rev. B* **52**, 803 (1995).
23. S. Semenovskaya, A.G. Khachaturyan, *Acta Mater.* **45**, 4367 (1997).
24. S. Semenovskaya, A.G. Khachaturyan, *J. Appl. Phys.* **83**, 5125 (1998).
25. E.K.H. Salje, *Phase Transitions in Ferroelastic and Co-Elastic Crystals* (Cambridge University Press, Cambridge, 1990).
26. K. Otsuka, C.M. Wayman, Eds., *Shape Memory Materials* (Cambridge University Press, Cambridge, 1998).
27. A. Planes, L. Mañosa, *Solid State Phys.* **55**, 159 (2001).
28. A. Saxena, T. Lookman, in *Handbook of Materials Modeling,* S. Yip, Ed. (Springer-Verlag, 2005), pp. 2143–2154.
29. S.R. Shenoy, T. Lookman, A. Saxena, A.R. Bishop, *Phys. Rev. B* **60**, R12537 (1999); K.O. Rasmussen, T. Lookman, A. Saxena, A.R. Bishop, R.C. Albers, S.R. Shenoy, *Phys. Rev. Lett.* **87**, 055704 (2001).
30. S.M. Shapiro, B.X. Yang, Y. Noda, L.E. Tanner, D. Schryvers, *Phys. Rev. B* **44**, 9301 (1991).
31. W. Cai, Y. Murakami, K. Otsuka, *Mater. Sci. Eng. A* **275**, 186 (1999).
32. T. Kakeshita, T. Fukuda, H. Tetsukawa, T. Saburi, K. Kindo, T. Takeuchi, M. Honda, S. Endo, T. Taniguchi, Y. Miyako, *Jpn. J. Appl. Phys.* **37**, 2535 (1998).
33. K. Otsuka, X. Ren, *Progr. Mater. Sci.* **50**, 511 (2005).
34. M.S. Choi, T. Fukuda, T. Kakeshita, H. Mori, *Philos. Mag.* **86**, 67 (2006).
35. W. Petry, *J. Phys. IV* **5**, C2–15 (1995).
36. J.S. Zhang, PhD thesis, University of Tsukuba, 2000.
37. Y. Wang, PhD thesis, Xi'an Jiaotong University, 2008.
38. V.K. Wadhawan, *Introduction to Ferroic Materials* (Gordon and Breach, Armsterdam, 2000).
39. D. Viehland, S.J. Jang, L.E. Cross, M. Wuttig, *Phys. Rev. B* **46**, 8003 (1992).
40. J.A. Mydosh, *Spin Glasses* (Taylor & Francis, London, 1993).
41. G. Burns, F.H. Dacol, *Phys. Rev. B* **28**, 2527 (1983).
42. Y. Murakami, D. Shindo, K. Oikawa, R. Kainuma, K. Ishida, *Acta Mater.* **50**, 2173 (2002). □

HORIBA
Scientific

No Matter the Game we Have an Easy Solution

Come see us at booth #801 at MRS Fall Meeting 2009

Featuring:

JOBIN YVON Technology

Find us at www.horiba.com/scientific or telephone:

USA:	+1-732-494-8660	France:	+33 (0)3 20 59 18 00
Germany:	+49 (0)62 51 84 750	UK:	+44 (0)20 8204 8142
Italy:	+39 02 57603050	Japan:	+81 (0)3 3861 8231
China:	+86 (0)10 8567 9966	Other Countries:	+33 (0)1 64 54 13 00

Look for our new e-mail addresses at HORIBA.com

Explore the future

Automotive Test Systems | Process & Environmental | Medical | Semiconductor | Scientific

HORIBA

Journals of material importance

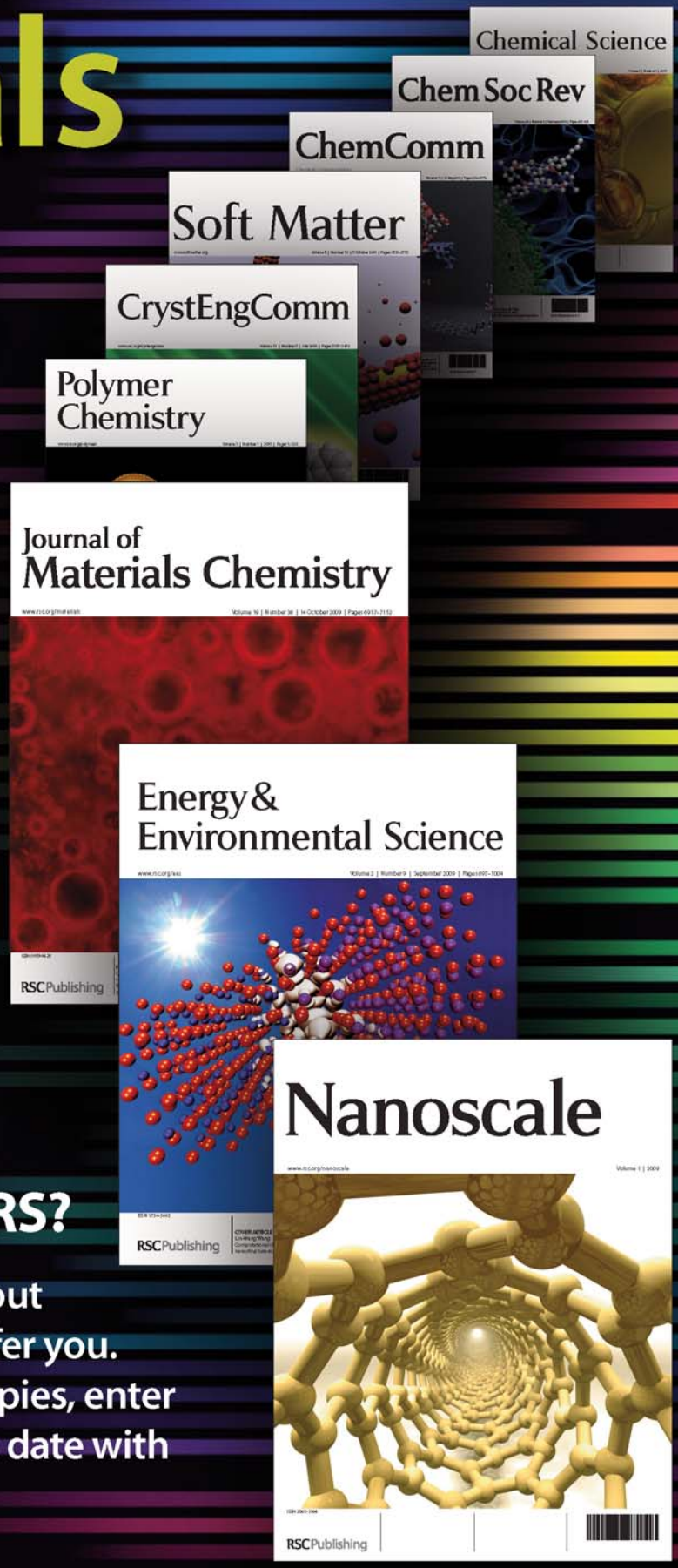

RSC journals are well known for their high scientific quality, impact, and fast publication times. At every stage from submission to publication, authors can rely on us to provide a first-class, professional publishing service.

Our rapidly expanding portfolio of materials products ensures that whatever the scope of your best research there is a high-quality home for it at the RSC. From weekly *Journal of Materials Chemistry* and other established titles like *Soft Matter* and *CrystEngComm*, to new journals *Energy & Environmental Science*, *Nanoscale* and *Polymer Chemistry*, plus flagship titles *ChemComm*, *Chem Soc Rev* and newly announced *Chemical Science*: we've got it covered.

Attending the Fall MRS?

Visit **Booth #114** to find out firsthand what the RSC can offer you. Pick up free sample journal copies, enter our prize draw and keep up to date with all the latest RSC news.

RSC Publishing

www.rsc.org/journals

Registered Charity Number 207890